NATIONAL ADVISORY COMMITTEE FOR AERONAUTICS

TECHNICAL NOTE 2777

THEORETICAL DISTRIBUTION OF SLIP ANGLES IN AN AGGREGATE OF FACE-CENTERED CUBIC CRYSTALS

By John M. Hedgepeth

Langley Aeronautical Laboratory
Langley Field, Va.

Washington
August 1952

1B

NATIONAL ADVISORY COMMITTEE FOR AERONAUTICS

TECHNICAL NOTE 2777

THEORETICAL DISTRIBUTION OF SLIP ANGLES IN AN AGGREGATE OF FACE-CENTERED CUBIC CRYSTALS

By John M. Hedgepeth

SUMMARY

An analysis of the relative frequency of occurrence of any given slip-line angle in a plastically deformed polycrystal composed of face-centered cubic crystals is presented for the case of simple tension. The results are compared with those obtained for a polycrystal composed of crystals which have but a single mode of slip and with experimental results. The comparisons show that the differences between the results obtained by the two theories become greater as the stress is increased. The comparison of the face-centered cubic theory with experiment is somewhat better than that of the single-slip-mode theory, but the errors are appreciable.

INTRODUCTION

The frequency distribution of the angular orientation of slip lines that are observed within separate grains on the surface of a plastically deformed polycrystal depends upon the detailed mechanism of plastic deformation. In reference 1 an attempt was made to assess quantitatively the assumptions on which the slip theory of plasticity (ref. 2) is based by investigating the implications of this theory concerning this frequency distribution. This assessment was made by comparing an experimental distribution with theoretical distributions calculated on the basis of the same model as that used in formulating the stress-strain laws of the slip theory. Although good agreement was obtained with regard to the shape of the distributions, the comparison between the experimental maximum slip angle and that predicted by theory was poor. One of the possible reasons for this poor comparison, as reported in reference 1, was the fact that the theory was based on a polycrystalline aggregate of grains which possess only one mode of slip; whereas aluminum, the metal used in the experiment, is made up of face-centered cubic crystals which have 12 modes of slip.

In order to investigate the quantitative effect of the multimode property of face-centered cubic crystals on the slip-angle distribution

an investigation was performed wherein this distribution was derived on the basis of the same assumptions as those used in reference 1 except that the grains were assumed to be face-centered cubic crystals instead of the single-slip-mode type. The theoretical derivations and the results of the investigation are presented herein.

SYMBOLS

$\bar{N}(\theta)$	cumulative probability of slipped grain having slip angle less than θ
$S(\theta)$	probability density of slipped grains having slip angle of θ
$G(\theta,\lambda)$	indicial cumulative probability
$K(\theta,\lambda)$	indicial probability density
$W(\lambda)$	weighting function (see eq. (7))
θ	slip angle
θ_{max}	maximum slip angle
$\lambda,\beta,\omega,\delta$	coordinates specifying orientation of slip-plane–direction combination with respect to specimen axis and viewing plane (see fig. 3)
x,y,z	coordinate axes (see fig. 3)
σ	tensile stress
σ_L	lowest value of tensile stress to cause slip
R	stress ratio, σ/σ_L
τ	resolved shear stress
τ_L	limit shear stress

THE FACE-CENTERED CUBIC CRYSTAL

The structure and distortion of the face-centered cubic crystal have been fully discussed in the literature (see, for example, refs. 3 to 5). For convenience, however, some of the characteristics of single crystals are given here.

Figure 1 indicates the basic slip systems of the crystal. In terms of the Miller indices (which are merely sets of direction numbers referred to the edges of the cube), the normals to the planes of slip are of the form $\{111\}$ (i.e. (111), $(1\bar{1}1)$, $(11\bar{1})$, etc.) and the slip directions in the plane are of the form $\langle 110 \rangle$ (i.e. $[110]$, $[1\bar{1}0]$, $[101]$, etc.). The octahedral planes therefore are the slip planes and the face diagonals are the slip directions. The regular tetrahedron shown inscribed in the cube contains the slip planes as faces and the slip directions as edges. Four slip planes and three slip directions in each plane produce a total of 12 possible plane-direction combinations or slip systems.

If a tensile stress σ is applied to a single crystal specimen along the specimen axis the resulting resolved shear stress on any particular slip system is given by

$$\tau = \sigma \cos \lambda \cos \delta \tag{1}$$

where λ and δ are the angles between the specimen axis and, respectively, the normal to the slip plane and the slip direction. This shear stress is, in general, different for each slip system in the crystal. The particular slip system for which τ has a maximum magnitude is, of course, dependent on the orientation of the crystal and can be found by comparing the shears on the various slip systems. The stereographic projection of the crystal shown in figure 2 summarizes the information obtained in reference 5 by such a comparison. The crystal is presumed to be fixed and the orientation of the crystal with respect to the loading direction is specified by the position of the specimen axis on the stereographic projection. The projection shows the orientation of the slip planes (of the form $\{111\}$, indicated by the symbol $\triangle$) and the slip directions (of the form $\langle 110 \rangle$, indicated by the symbol $\bigcirc$) with respect to the orientation of the cube edges (of the form $\langle 100 \rangle$, indicated by the symbol $\square$). The great-circle arcs connecting the various directions divide the hemisphere into 24 equal triangular regions. The set of indices within each region expresses the particular slip plane (upper indices) and slip direction (lower indices) most highly loaded if the specimen axis falls within that region. Since the resolved shear stress required to cause slip along any given slip system of a virgin crystal is independent of the orientation of the slip system, the sets of indices also denote the particular slip system which will initially undergo slip. (An exception to this statement is noted in ref. 6 wherein the required resolved shear stress is found to be different for different slip systems in a thin, plate-like crystal.) As the crystal is loaded further in tension the same slip system will continue to undergo slip provided the crystallographic orientation remains essentially unchanged with respect to the

loading direction; the other systems will remain dormant because, as has been shown experimentally, the dormant slip systems are strain-hardened to at least the same extent as the operative ones. (See ref. 3, p. 304.)

THEORY

In the derivation a polycrystalline specimen is considered to be plastically strained in tension. The grains, which are so oriented that the resolved shear stress on the most highly loaded slip-plane–direction combination is sufficiently great, exhibit slip along the slip plane which is evidenced in the form of slip lines on the surface of the specimen. If the specimen axis is vertical, the slip lines are inclined to the horizontal at various angles known as slip angles. As in reference 1 the objective is the calculation of the relative frequency of occurrence of slipped grains with various slip angles.

The desired result can be expressed, in one way, as a cumulative probability, that is, as the relative number of slipped grains having slip angles less than a given value. This cumulative probability $\bar{N}(\theta)$ can be found conceptually by counting the slipped grains with slip angles less than θ and dividing by the total number of slipped grains. Another way to express the desired result is as a frequency distribution or probability density, that is, as the relative density of slipped grains with a given slip angle. The probability density $S(\theta)$ is found to be equal to the derivative of $\bar{N}(\theta)$ with respect to θ. Both of these quantities are derived herein.

The following assumptions, which with the exception of assumption 2 are common to those used in reference 1, are used in the derivation:

(1) The crystallographic orientation of the grains in the specimen is random.

(2) The specimen is composed of face-centered cubic crystals.

(3) The microscopic stress state in each grain in the same as the macroscopic stress on the specimen as a whole.

(4) A grain slips when the resolved shear stress in the slip direction in the slip plane is greater than a certain limiting value, herein called the limit shear stress, which is the same for all grains.

The model thus consists of a specimen composed of a very large number of randomly oriented grains of identical crystallographic properties subjected to a common tensile stress in the direction of the

specimen axis. In the determination of the slip-angle distribution, the following questions must be answered for each particular grain:

(1) Which is the most highly loaded slip system?

(2) Does this system undergo slip? In other words, is the resolved shear stress greater than the limit shear stress?

(3) If slip occurs, what is the slip angle produced?

With these questions answered for each grain the relative frequency of occurrence of slipped grains with the various slip angles can be determined. Now, the concept of having many randomly oriented grains can be replaced by the concept of having a single grain which is allowed to assume randomly all orientations; each different orientation represents a different grain. Furthermore, since the 12 slip systems are crystallographically equivalent, attention can be directed to only those orientations for which a particular slip system (say the $(111/0\bar{1}1)$ system) would be most highly loaded. If the orientation is such that another slip system is most highly loaded, the basic tetrahedron of figure 1 can be rotated to bring the $(111/0\bar{1}1)$ system into coincidence with this most highly loaded system and this new orientation will be crystallographically the same as the old. By means of this artificial restriction of the orientation the first question is automatically answered and only the second and third questions need to be answered.

In order to answer these questions, the orientation of each crystal with respect to both the specimen axis and the viewing plane must be specified. One method of specification was used in reference 1 wherein the specimen axis and viewing plane were fixed and the orientation of the grain was allowed to vary. A better method for the purposes of this analysis would be to hold the grain fixed and allow the orientation of the specimen axis and viewing plane to vary. The quantities necessary to specify these orientations are shown in figure 3 wherein the (111) plane is the xy-plane and the $[0\bar{1}1]$ direction is the x-axis. The orientation of the specimen axis is given by the spherical coordinates λ, the angle between the specimen axis and the normal to the slip plane, and β, the angle between the slip direction and plane OAC which passes through the specimen axis and is normal to the slip plane. The orientation of the viewing plane (which is, of course, parallel to the specimen axis) is given by ω, the complement of the dihedral angle between the viewing plane OAB and the aforementioned plane OAC. The slip line produced by the intersection of the slip and viewing planes and the slip angle θ, the angle measured in the viewing plane between the slip line and the normal to the specimen axis, are also shown in figure 3. These quantities defining the orientation are exactly equivalent to those used in reference 1.

The value of ω is in no way involved in answering the question of whether a grain will slip; variation of ω merely changes the slip angle produced and only the values of λ and β need to be known to answer this question. If the stereographic projection shown in figure 2 is rotated to bring the normal to the $(\bar{1}11)$ plane into the center, the projection in figure 4 is produced. In figure 4 only those parts of the projection which will be useful are shown. As was previously remarked, the only orientations of the grain that are considered are those for which the slip system $(111/0\bar{1}1)$ is most highly loaded. The triangular region specifying orientations of the specimen axis (or values of λ and β as indicated in fig. 4) for which this slip system is most highly loaded is therefore shown. Thus, the restricting condition is merely that only values of λ and β within this triangle are to be considered. This limitation entirely takes into account the multimode property of the face-centered cubic crystal and constitutes the significant difference between multimode and single-mode crystals; there would be no restriction of values of λ and β for a single-mode crystal.

The question of whether a grain will slip can now be answered. The resolved shear stress on the $(111/0\bar{1}1)$ slip system due to a tensile stress σ along the specimen axis is given by

$$\tau = \sigma \cos \lambda \sin \lambda \cos \beta \tag{2}$$

The locus of positions of the specimen axis for which $\tau = \tau_L$, the limit shear stress, is given by

$$\tau_L = \sigma \cos \lambda \sin \lambda \cos \beta$$

or

$$\frac{1}{R} = \sin 2\lambda \cos \beta \tag{3}$$

where R is the stress ratio and is equal to $\frac{\sigma}{\sigma_L}$ in which $\sigma_L = 2\tau_L$.

For a fixed value of R, equation (3) describes a closed curve such as that shown in figure 4 which separates the sphere into two regions, the one inside being where $\tau > \tau_L$ and the one outside being where $\tau < \tau_L$. As R is increased the curve encompasses an ever widening region starting with a point at $\lambda = \frac{\pi}{4}$, $\beta = 0$ for $R = 1$ and increasing to

the whole region $0 < \lambda < \frac{\pi}{2}$, $-\frac{\pi}{2} < \beta < \frac{\pi}{2}$ for $R = \infty$. Such curves and regions have been constructed by Von Göler and Sachs (see, for example, ref. 4, p. 38) for a different orientation of the basic triangle than the one contained herein.

For a grain to slip at a given stress ratio the grain must be oriented so that the specimen axis falls in this region. In addition, however, a restrictive condition is that the specimen axis must fall within the spherical triangle. The specimen axis thus must be included both in this region and the spherical triangle. For small values of R the curve for $\tau = \tau_L$ falls entirely within the triangle and the results should be the same as those obtained in reference 1 because the restrictive condition is not involved. For large values of R the curve lies entirely without the triangle and the exact value of the stress ratio is unimportant; the value of R is high enough to cause slip in all the grains and the slip-angle distribution is frozen. At intermediate values of R both the triangular boundary and the value of the stress ratio are important.

Attention up to this point in the discussion has been directed mainly to considering the variables λ and β. Variation of ω, as was pointed out, only changes the slip angle produced. The effect of ω is taken into account in the following manner. Define the indicial cumulative probability $G(\lambda,\theta)$ as the probability of a slipped grain, the orientation of which with respect to the specimen axis is given by λ and β, exhibiting a slip angle less than θ. (This indicial cumulative probability is independent of β, as will be seen later.) The equation for $\overline{N}(\theta)$ can then be obtained by superposition:

$$\overline{N}(\theta) = \frac{\iint_A G(\lambda,\theta)\sin\lambda \, d\lambda \, d\beta}{\iint_A \sin\lambda \, d\lambda \, d\beta} \tag{4}$$

where the quantity $\sin\lambda \, d\lambda \, d\beta$ is an elemental area on the sphere shown in figure 4, and the integrations in both the numerator and the denominator are carried out over the area A which is included both within the spherical triangle and the curve $\tau = \tau_L$. The numerator thus is effectively the sum of the indicial cumulative probabilities for each position of the specimen axis (λ,β) over all positions which produce slip, and the denominator is effectively the sum of all positions (λ,β) which produce slip.

In order to derive the expression for $G(\lambda,\theta)$, the relationship between the orientation of the slip system (given by $(\lambda,\beta,\omega,)$) and θ must be known. This relationship can be obtained from figure 3 by solving the irregular tetrahedron OABC and is

$$\sin \omega = \frac{\tan \theta}{\tan \lambda} \tag{5}$$

Note that the value of β does not enter into this relationship since the slip angle produced by slip on a given system depends only on the orientation of the slip plane and not on the direction of slip within the plane. Because of the symmetry of this equation only values of ω between zero and $\pi/2$ need be considered in the calculation of $G(\lambda,\theta)$. The quantity $G(\lambda,\theta)$ is by definition the proportion of all values of ω in this range for which the slip angle is less than a given value of θ. When $\lambda < \theta$, the slip angle produced will be less than θ for all values of ω; when $\lambda > \theta$, the slip angle produced will be less than θ for all values of ω between 0 and $\sin^{-1}(\tan \theta/\tan \lambda)$. Thus,

$$\left.\begin{aligned} G(\lambda,\theta) &= 1 && (\lambda < \theta) \\ &= \frac{2}{\pi} \sin^{-1} \frac{\tan \theta}{\tan \lambda} && (\lambda > \theta) \end{aligned}\right\} \tag{6}$$

Note that the indicial cumulative probability is independent of β as a consequence of the fact that β does not appear in equation (5). Since the limits on the β-integrations in equation (4) are functions only of λ, the expression for $\overline{N}(\theta)$ can be written

$$\overline{N}(\theta) = \frac{\int_0^{\pi/2} W(\lambda)G(\lambda,\theta)\sin \lambda \, d\lambda}{\int_0^{\pi/2} W(\lambda)\sin \lambda \, d\lambda} \tag{7}$$

In this expression, the term $W(\lambda)$ is merely the difference between the values of β at the end points of the small circle with radius λ which is included in both the triangular area and the region inside the curve $\tau = \tau_L$. The value of $W(\lambda)$ is zero for values of λ for which there are no positions of the specimen axis within both of these regions. The expression for the probability density $S(\theta)$ can be obtained by taking the derivative of $\overline{N}(\theta)$ with respect to θ

$$S(\theta) = \frac{\int_0^{\pi/2} W(\lambda)K(\lambda,\theta)\sin\lambda\, d\lambda}{\int_0^{\pi/2} W(\lambda)\sin\lambda\, d\lambda} \tag{8}$$

where

$$\left.\begin{aligned} K(\lambda,\theta) &= \frac{d}{d\theta} G(\lambda,\theta) \\ &= 0 \qquad (\lambda < \theta) \\ &= \frac{2}{\pi} \frac{\sec^2\theta}{\sqrt{\tan^2\lambda - \tan^2\theta}} \qquad (\lambda > \theta) \end{aligned}\right\} \tag{9}$$

In equations (7) and (8), the function $W(\lambda)$ can be interpreted as being a weighting function used in the superposition of the indicial cumulative probability $G(\lambda,\theta)$ and the indicial probability density $K(\lambda,\theta)$. In order to determine the end-point values of β for the purpose of calculating $W(\lambda)$, use must be made of equation (3) as well as the equations of the great circles bounding the triangular area; these equations are obtained in the appendix and the results are summarized here. (Each great circle is denoted by the points through which it passes.)

For great circle (001,101),

$$\beta = \frac{\pi}{6} - \cos^{-1}\frac{\cot\lambda}{\sqrt{2}} \tag{10a}$$

For great circle $(001,1\bar{1}1)$,

$$\beta = \cos^{-1}\left(\sqrt{2}\cot\lambda\right) - \frac{\pi}{6} \tag{10b}$$

For great circle $(101,1\bar{1}1)$,

$$\beta = \frac{\pi}{6} \tag{10c}$$

As can be expected, for a fixed value of R, the variable λ must be separated into various ranges in the determination of $W(\lambda)$. In addition, the stress ratio itself must be separated into various ranges. A discussion of each range of R and illustrative sketches follow:

(1) Range I: $1 < R < \frac{\sqrt{6}}{1 + \sqrt{2}}$

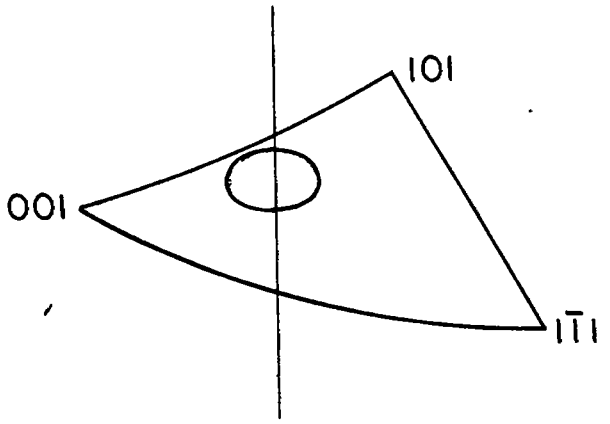

In this range the curve for $\tau = \tau_L$ falls entirely within the triangle; the upper limit of this range is the value of R for which the curve $\tau = \tau_L$ first touches the great circle (001,101). The values of $W(\lambda)$ are

$$\left.\begin{aligned} W(\lambda) &= 0 && (0 < \lambda < \lambda_1) \\ &= 2 \cos^{-1} \frac{1}{R \sin 2\lambda} && (\lambda_1 < \lambda < \lambda_2) \\ &= 0 && \left(\lambda_2 < \lambda < \frac{\pi}{2}\right) \end{aligned}\right\} \tag{11}$$

where the minimum and maximum values of λ on the curve $\tau = \tau_L$ are

$$\lambda_1 = \frac{1}{2} \sin^{-1} \frac{1}{R}$$

$$\lambda_2 = \frac{\pi}{2} - \frac{1}{2} \sin^{-1} \frac{1}{R}$$

(2) Range II: $\frac{\sqrt{6}}{1 + \sqrt{2}} < R' < \frac{5}{2\sqrt{6}}$

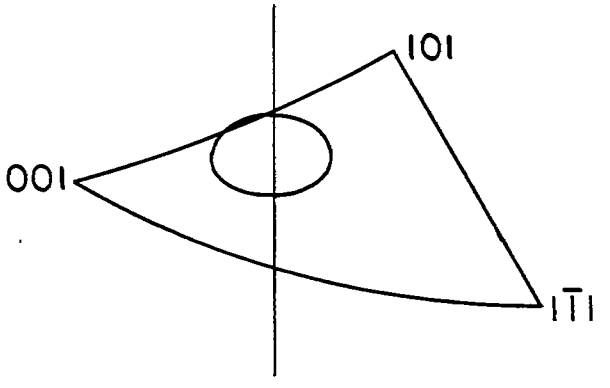

In this range and in subsequent ranges both the curve and the triangle are involved. The upper limit of this range is the value of R for which the curve intersects the great circle (001,101) at $\beta = 0$. The values of $W(\lambda)$ are

$$
W(\lambda) = \begin{cases}
0 & (0 < \lambda < \lambda_1) \\
2 \cos^{-1} \dfrac{1}{R \sin 2\lambda} & (\lambda_1 < \lambda < A_1) \\
\cos^{-1} \dfrac{1}{R \sin 2\lambda} + \cos^{-1} \dfrac{\cot \lambda}{\sqrt{2}} - \dfrac{\pi}{6} & (A_1 < \lambda < A_2) \\
2 \cos^{-1} \dfrac{1}{R \sin 2\lambda} & (A_2 < \lambda < \lambda_2) \\
0 & \left(\lambda_2 < \lambda < \dfrac{\pi}{2}\right)
\end{cases} \tag{12}
$$

where the values of λ at the intersections between the curve for $\tau = \tau_L$ and the great circle (001,101) are

$$A_{1,2} = \frac{1}{2} \cos^{-1} \frac{\frac{\sqrt{6}}{R} - 2 \pm \sqrt{1 + \frac{2\sqrt{6}}{R} - \frac{6}{R^2}}}{3}$$

(3) Range III: $\dfrac{5}{2\sqrt{6}} < R < \dfrac{6}{3 + \sqrt{6}}$

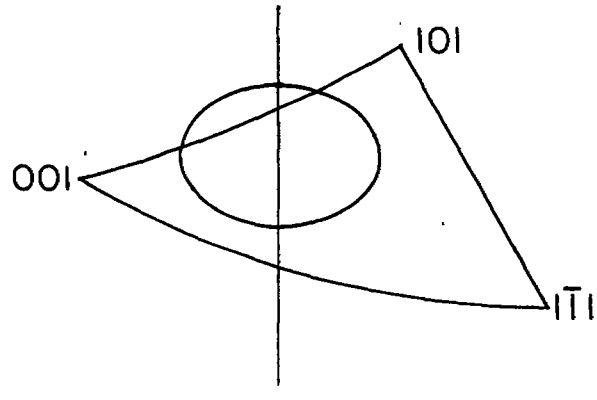

The upper limit of this range is the value of R for which the curve first touches the great circle $(001,1\bar{1}1)$. The values of $W(\lambda)$ are

$$\left.\begin{aligned} W(\lambda) &= 0 && (0 < \lambda < A_1) \\ &= \cos^{-1}\frac{1}{R \sin 2\lambda} + \cos^{-1}\frac{\cot\lambda}{\sqrt{2}} - \frac{\pi}{6} && (A_1 < \lambda < A_2) \\ &= 2\cos^{-1}\frac{1}{R \sin 2\lambda} && (A_2 < \lambda < \lambda_2) \\ &= 0 && \left(\lambda_2 < \lambda < \frac{\pi}{2}\right) \end{aligned}\right\} \quad (13)$$

(4) Range IV: $\dfrac{6}{3+\sqrt{6}} < R < \dfrac{11}{4\sqrt{6}}$

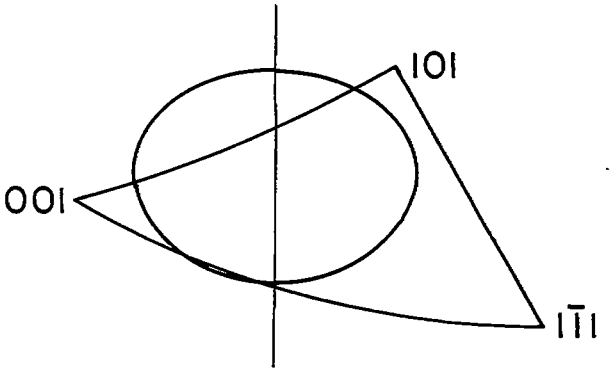

The maximum value of R in this range is that for which the intersection between the curve and the great circle $(001,1\bar{1}1)$ occurs at $\beta = 0$. The values of $W(\lambda)$ are

$$
\left.
\begin{aligned}
W(\lambda) &= 0 && (0 < \lambda < A_1) \\
&= \cos^{-1}\frac{1}{R \sin 2\lambda} + \cos^{-1}\frac{\cot\lambda}{\sqrt{2}} - \frac{\pi}{6} && (A_1 < \lambda < A_2) \\
&= 2\cos^{-1}\frac{1}{R \sin 2\lambda} && (A_2 < \lambda < B_1) \\
&= \cos^{-1}\frac{1}{R \sin 2\lambda} - \cos^{-1}\left(\sqrt{2}\cot\lambda\right) + \frac{\pi}{6} && (B_1 < \lambda < B_2) \\
&= 2\cos^{-1}\frac{1}{R \sin 2\lambda} && (B_2 < \lambda < \lambda_2) \\
&= 0 && \left(\lambda_2 < \lambda < \frac{\pi}{2}\right)
\end{aligned}
\right\} \quad (14)
$$

where the values of λ at the intersections between the curve for $\tau = \tau_L$ and the great circle $(001,1\bar{1}1)$ are

$$
B_{1,2} = \frac{1}{2}\cos^{-1}\frac{\frac{2\sqrt{6}}{R} - 8 \pm \sqrt{1 + \frac{4\sqrt{6}}{R} - \frac{12}{R^2}}}{9}
$$

(5) Range V: $\frac{11}{4\sqrt{6}} < R < \frac{2}{\sqrt{3}}$

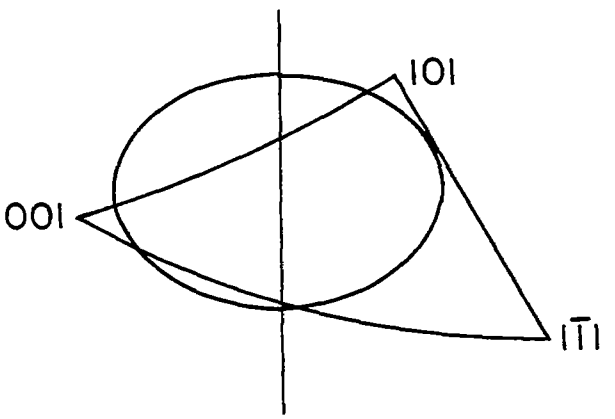

The upper limit of this range is given by the value of R for which the curve first touches the great circle (101,1$\bar{1}$1). The values of $W(\lambda)$ are

$$
\left.
\begin{aligned}
W(\lambda) &= 0 && (0 < \lambda < A_1) \\
&= \cos^{-1}\frac{1}{R \sin 2\lambda} + \cos^{-1}\frac{\cot\lambda}{\sqrt{2}} - \frac{\pi}{6} && (A_1 < \lambda < A_2) \\
&= 2\cos^{-1}\frac{1}{R \sin 2\lambda} && (A_2 < \lambda < B_1) \\
&= \cos^{-1}\frac{1}{R \sin 2\lambda} - \cos^{-1}\left(\sqrt{2}\cot\lambda\right) + \frac{\pi}{6} && (B_1 < \lambda < B_2) \\
&= 0 && \left(B_2 < \lambda < \frac{\pi}{2}\right)
\end{aligned}
\right\} \quad (15)
$$

(6) Range VI: $\frac{2}{\sqrt{3}} < R < \sqrt{\frac{3}{2}}$

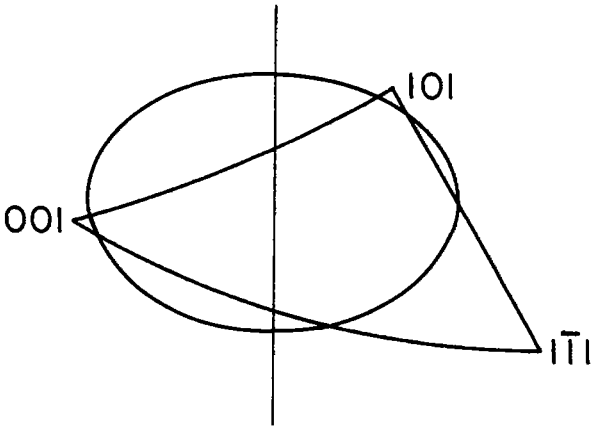

The maximum value of R in this range is that for which the curve passes (simultaneously) through both the corners (001) and (101). The values of $W(\lambda)$ are

$$
\left.
\begin{aligned}
W(\lambda) &= 0 && (0 < \lambda < A_1)\\
&= \cos^{-1}\frac{1}{R \sin 2\lambda} + \cos^{-1}\frac{\cot\lambda}{\sqrt{2}} - \frac{\pi}{6} && (A_1 < \lambda < C_1)\\
&= \cos^{-1}\frac{\cot\lambda}{\sqrt{2}} && (C_1 < \lambda < C_2)\\
&= \cos^{-1}\frac{1}{R \sin 2\lambda} + \cos^{-1}\frac{\cot\lambda}{\sqrt{2}} - \frac{\pi}{6} && (C_2 < \lambda < A_2)\\
&= 2\cos^{-1}\frac{1}{R \sin 2\lambda} && (A_2 < \lambda < B_1)\\
&= \cos^{-1}\frac{1}{R \sin 2\lambda} - \cos^{-1}\left(\sqrt{2}\cot\lambda\right) + \frac{\pi}{6} && (B_1 < \lambda < B_2)\\
&= 0 && \left(B_2 < \lambda < \frac{\pi}{2}\right)
\end{aligned}
\right\} \quad (16)
$$

where the intersections between the curve for $\tau = \tau_L$ and the great circle $(101,1\bar{1}1)$ are

$$C_1 = \frac{1}{2} \sin^{-1} \frac{2}{\sqrt{3}R}$$

$$C_2 = \frac{\pi}{2} - \frac{1}{2} \sin^{-1} \frac{2}{\sqrt{3}R}$$

(7) Range VII: $\sqrt{\frac{3}{2}} < R < \frac{3}{2}\sqrt{\frac{3}{2}}$

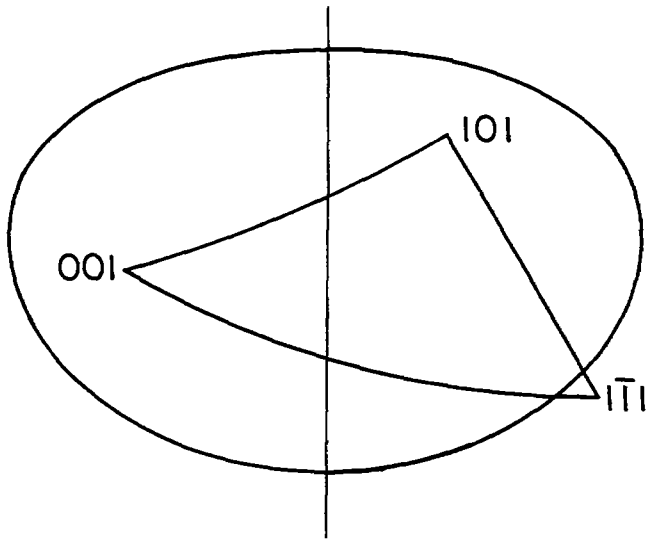

The upper limit of this range is the value of R for which the curve passes through the corner $(1\bar{1}1)$. The values of $W(\lambda)$ are

$$
W(\lambda) = \begin{cases}
0 & \left(0 < \lambda < \cos^{-1}\sqrt{\frac{2}{3}}\right) \\
\cos^{-1}\dfrac{\cot\lambda}{\sqrt{2}} & \left(\cos^{-1}\sqrt{\frac{2}{3}} < \lambda < \cos^{-1}\sqrt{\frac{1}{3}}\right) \\
\dfrac{\pi}{3} - \cos^{-1}\left(\sqrt{2}\cot\lambda\right) & \left(\cos^{-1}\sqrt{\frac{1}{3}} < \lambda < C_2\right) \\
\cos^{-1}\dfrac{1}{R\sin 2\lambda} - \cos^{-1}\left(\sqrt{2}\cot\lambda\right) + \dfrac{\pi}{6} & (C_2 < \lambda < B_2) \\
0 & \left(B_2 < \lambda < \frac{\pi}{2}\right)
\end{cases} \tag{17}
$$

(8) Range VIII: $\frac{3}{2}\sqrt{\frac{3}{2}} < R$

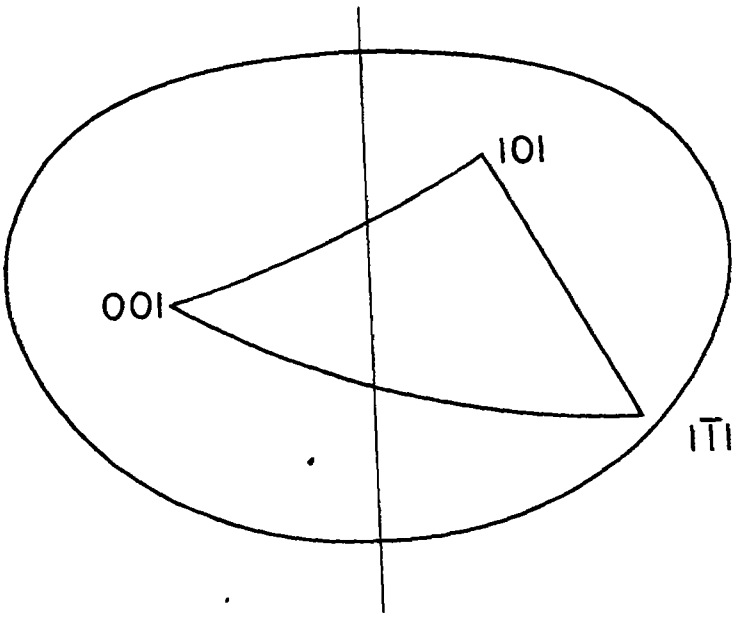

In this last range the curve lies outside the triangle and the exact value of R is unimportant; slip occurs in all grains and the slip-angle distribution is frozen. The values of $W(\lambda)$ are

$$\left.\begin{aligned} W(\lambda) &= 0 && \left(0 < \lambda < \cos^{-1}\sqrt{\frac{2}{3}}\right) \\ &= \cos^{-1}\frac{\cot\lambda}{\sqrt{2}} && \left(\cos^{-1}\sqrt{\frac{2}{3}} < \lambda < \cos^{-1}\sqrt{\frac{1}{3}}\right) \\ &= \frac{\pi}{3} - \cos^{-1}\left(\sqrt{2}\cot\lambda\right) && \left(\cos^{-1}\sqrt{\frac{1}{3}} < \lambda < \cos^{-1}\frac{1}{3}\right) \\ &= 0 && \left(\cos^{-1}\frac{1}{3} < \lambda < \frac{\pi}{2}\right) \end{aligned}\right\} \quad (18)$$

The theoretical derivation is thus completed. By using equations (11) to (18) in conjunction with equations (6) and (9), the cumulative probability $N(\theta)$ (eq. (7)) and the probability density $S(\theta)$ (eq. (8)) can be evaluated.

RESULTS AND COMPARISONS

In order to show the difference between the results obtained herein and those derived in reference 1 the curves for $\overline{N}(\theta)$ and $S(\theta)$ have been computed by both theories for three values of R and compared in figures 5 to 7. In the calculation of these curves, the integrations necessary for computing $S(\theta)$ were carried out numerically. For isolated cases, however, the integrals could be expressed in the form of elliptic functions and these exact evaluations were used as a check. The curves for $\overline{N}(\theta)$ were found by numerically integrating the curves for $S(\theta)$, $S(\theta)$ being the derivative of $\overline{N}(\theta)$ with respect to θ. As can be seen from figure 5 for which R = 1.015, there is no plottable difference between the results for this value of stress ratio. When the stress ratio is increased to 1.156, the effect, as shown in figure 6, increases appreciably. Even more effect is apparent in figure 7, for which the stress ratio is 1.837. It should be noted that the value of the stress ratio R = 1.837 is the one for which the slip-angle distribution derived in the present paper becomes frozen. For higher values of the stress ratio the curves for the face-centered cubic distributions would be the same as those shown in figure 7, whereas the curves derived on the basis of single-mode crystals would continue to change.

The manner in which the differences between the two theories exhibit themselves can be seen from figures 5 to 7. The values of $S(\theta)$ for the single-mode crystal remain almost constant for low values of θ as the stress ratio is changed; whereas the corresponding values for the face-centered cubic crystal decrease as R is increased (until $R = 1.837$, of course). The value of slip angle where the probability density is maximum continually decreases as the stress ratio is increased for the single-mode crystals; whereas the value for which the maximum is obtained remains at about 45° for the face-centered cubic crystal. The value of the maximum slip angle, denoted herein by θ_{max}, for the face-centered cubic crystal is always less than or equal to θ_{max} for the single-mode crystal.

More detailed consideration can be given to this last point. It was found in reference 1 that θ_{max} is, for single-mode crystals, equal to λ_2. The value of θ_{max} as obtained herein is clearly given by the maximum value of λ for which $W(\lambda)$ is not zero. (See eqs. (8) and (9).) Thus, for face-centered cubic crystals,

$$\theta_{max} = \lambda_2 \qquad \left(R < \frac{11}{4\sqrt{6}}\right)$$

$$= B_2 \qquad \left(\frac{11}{4\sqrt{6}} < R < \frac{3}{2}\sqrt{\frac{3}{2}}\right)$$

$$= \cos^{-1}\frac{1}{3} \qquad \left(\frac{3}{2}\sqrt{\frac{3}{2}} < R\right)$$

These results for θ_{max} are plotted against the stress ratio R in figure 8. For comparison the corresponding results for the single-mode theory are also shown.

In reference 1 an experimentally obtained slip-angle distribution was shown. This distribution was taken from a photomicrograph of a polished 2S-0 aluminum alloy specimen at 0.022 strain. At this strain, the stress ratio was found to be approximately 2 and, in addition, the stress was high enough to cause slip in all the grains. The experimental distribution is plotted in figure 9 along with the face-centered-cubic frozen distribution and the single-mode distribution for $R = 2.000$ taken from reference 1. The comparison is somewhat better between the experiment and the face-centered cubic theory than between the experiment and the single-mode theory. At the higher slip angles, however, the agreement is still not very close. In particular,

the maximum experimental slip angle of 58° is still far below that predicted by the face-centered cubic theory (70° 32'). It is a point of interest that the analysis of other photomicrographs of similar specimens strained in the same manner as the specimen from which this experimental distribution was obtained has yielded no slip lines with slip angles greater than 63°. Thus experience has shown that there is an utter lack of slip angles between 63° and the theoretical 70° 32' in polycrystals that have been strained in tension until all the grains have slipped. It might be argued that the reason for this lack is due to the small theoretical probability of a grain exhibiting a slip angle between, say, 58° and 70° 32' (on the order of 0.05), but a simple calculation shows that the probability of at least one of 123 grains (which is the size of the sample from which the distribution shown in fig. 9 was obtained) exhibiting a slip angle between 58° and 70° 32' is

$$1 - (1 - 0.05)^{123}$$

or 0.998, almost a certainty. Some other reason must therefore exist for the aforementioned lack. This reason is undoubtedly connected with either the fact that surface grains do not act like interior ones or the violation of one of the assumptions. With regard to this latter point, the assumption dealing with equality of microscopic and macroscopic stresses seems to be the most likely suspect, particularly since it is generally agreed that the stress state in a polycrystal varies from grain to grain. (See, for example, ref. 7.)

CONCLUDING REMARKS

The differences between theoretical slip-angle distributions derived on the basis of polycrystal aggregates made up of single-slip-mode crystals and those made up of face-centered cubic crystals are found to be appreciable, the difference increasing as the stress is increased.

The face-centered cubic theory agrees somewhat better with experiment than the single-mode theory, but the errors are still appreciable. These errors are probably due to the inadequacy of the assumption involving the homogeneity of stress from grain to grain.

Langley Aeronautical Laboratory
National Advisory Committee for Aeronautics
Langley Field, Va., June 20, 1952

APPENDIX

EQUATIONS OF GREAT CIRCLES BOUNDING THE TRIANGLE OF INTEREST

In order to obtain analytical results for $W(\lambda)$ the equations of the great circles bounding the triangle shown in figure 4 must be known. The approach that is used in this analysis is to find first the general equation of a great circle and then to fit the equation to the points through which each bounding circle must pass.

In terms of the coordinates λ,β in figure 3, the direction cosines of a given direction (or a given point on the sphere from which the stereographic projection is obtained) with respect to the x-, y-, and z-axes are

$$l_x,\ l_y,\ l_z = \sin\lambda\cos\beta,\ \ \sin\lambda\sin\beta,\ \ \cos\lambda \tag{A1}$$

A great circle can be defined, in one way, as the locus of points on the sphere that are 90° away from a fixed point called the pole of the great circle. If the location of the pole of a great circle is denoted by λ_0,β_0 with the direction cosines $l_{x_0},\ l_{y_0},\ l_{z_0}$, the points on the great circle must satisfy the equation

$$l_x l_{x_0} + l_y l_{y_0} + l_z l_{z_0} = 0$$

or

$$\sin\lambda\sin\lambda_0\cos(\beta - \beta_0) + \cos\lambda\cos\lambda_0 = 0$$

or

$$\beta = \beta_0 + \cos^{-1}(-\cot\lambda\cot\lambda_0) \tag{A2}$$

Equation (A2) is the general equation for a great circle. The equation has two unknown constants, β_0 and $\cot\lambda_0$. These constants can be determined from the coordinates of two points through which the great circle is known to pass. The corners of the spherical triangle shown in figure 4 furnish the necessary points.

The coordinates of the corners can be found from the angles between the corners and the known points (111) and $(0\bar{1}1)$. Since the Miller indices of the various directions are direction numbers referred to a common set of axes, these angles can be easily determined. For instance, the cosine of the angle between the (111) point and the (101) point is given by

$$\left(\frac{1}{\sqrt{3}}\right)\left(\frac{1}{\sqrt{2}}\right) + \left(\frac{1}{\sqrt{3}}\right)(0) + \left(\frac{1}{\sqrt{3}}\right)\left(\frac{1}{\sqrt{2}}\right) = \sqrt{\frac{2}{3}}$$

and the cosine of the angle between the $(0\bar{1}1)$ point and the (101) point is given by

$$(0)\left(\frac{1}{\sqrt{2}}\right) - \left(\frac{1}{\sqrt{2}}\right)(0) + \left(\frac{1}{\sqrt{2}}\right)\left(\frac{1}{\sqrt{2}}\right) = \frac{1}{2}$$

Knowledge of these two angles allows the determination of the coordinates of the point (101). Thus

$$(\sin \lambda \cos \beta)(0) + (\sin \lambda \sin \beta)(0) + (\cos \lambda)(1) = \sqrt{\frac{2}{3}}$$

$$(\sin \lambda \cos \beta)(1) + (\sin \lambda \sin \beta)(0) + (\cos \lambda)(0) = \frac{1}{2}$$

therefore,

$$\cos \lambda = \sqrt{\frac{2}{3}}$$

and

$$\beta = \frac{\pi}{6} .$$

Similarly, the coordinates of the other two corners can be determined to be

$$\left.\begin{aligned}\cos\lambda &= \frac{1}{3}\\ \beta &= \frac{\pi}{6}\end{aligned}\right\} \text{ for the corner } (1\bar{1}1)$$

and

$$\left.\begin{aligned}\cos\lambda &= \sqrt{\frac{1}{3}}\\ \beta &= -\frac{\pi}{6}\end{aligned}\right\} \text{ for the corner } (001)$$

In order that each bounding great circle pass through the required points the arbitrary constants in equation (A2) must be such that the resulting equations are:

For great circle (001,101),

$$\beta = \frac{\pi}{6} - \cos^{-1}\frac{\cot\lambda}{\sqrt{2}} \tag{A3a}$$

For great circle (001,1$\bar{1}$1),

$$\beta = \cos^{-1}\left(\sqrt{2}\cot\lambda\right) - \frac{\pi}{6} \tag{A3b}$$

For great circle (101,1$\bar{1}$1),

$$\beta = \frac{\pi}{6} \tag{A3c}$$

REFERENCES

1. Hedgepeth, John M., Batdorf, S. B., and Sanders, J. Lyell, Jr.: On the Angular Distribution of Slip Lines in Polycrystalline Aluminum Alloy. NACA TN 2577, 1951.

2. Batdorf, S. B., and Budiansky, Bernard: A Mathematical Theory of Plasticity Based on the Concept of Slip. NACA TN 1871, 1949.

3. Barrett, Charles S.: Structure of Metals. McGraw-Hill Book Co., Inc., 1943.

4. Elam, C. F.: Distortion of Metal Crystals. Oxford Univ. Press, 1935.

5. Taylor, G. I., and Elam, C. F.: The Plastic Extension and Fracture of Aluminium Crystals. Proc. Roy. Soc. (London), ser. A, vol. 108, 1925, pp. 28-51.

6. Wu, T. L., and Smoluchowski, R.: A New Criterion for the Occurrence of Slip in Thin Single Crystals. Phys. Rev., vol. 78, no. 4, Second ser., May 15, 1950, pp. 468-469.

7. Boas, W., and Hargreaves, M. E.: On the Inhomogeneity of Plastic Deformation in the Crystals of an Aggregate. Proc. Roy. Soc. (London), ser. A, vol. 193, no. 1032, Apr. 22, 1948, pp. 89-97.

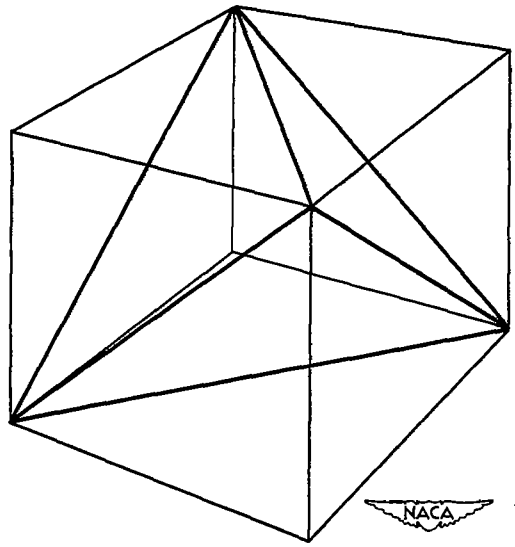

Figure 1.- Slip systems of the face-centered cubic crystal.

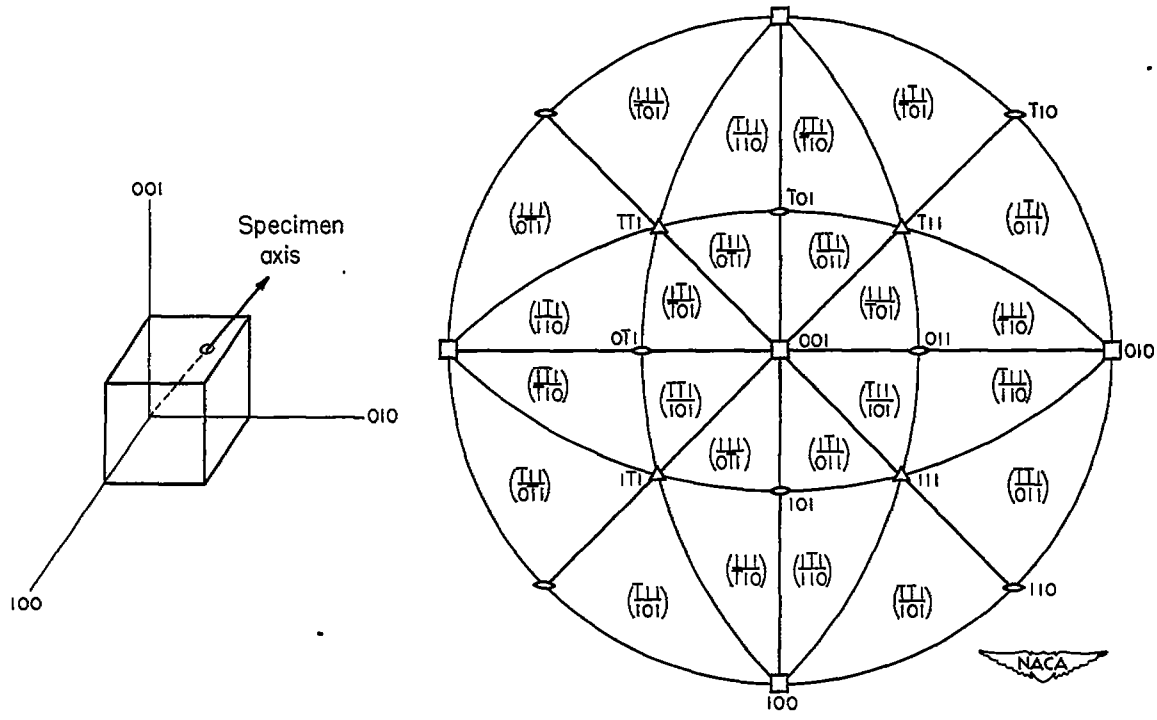

Figure 2.- Stereographic projection for obtaining the most highly loaded slip system for a known orientation. The numbers within each region indicate the most highly loaded slip system.

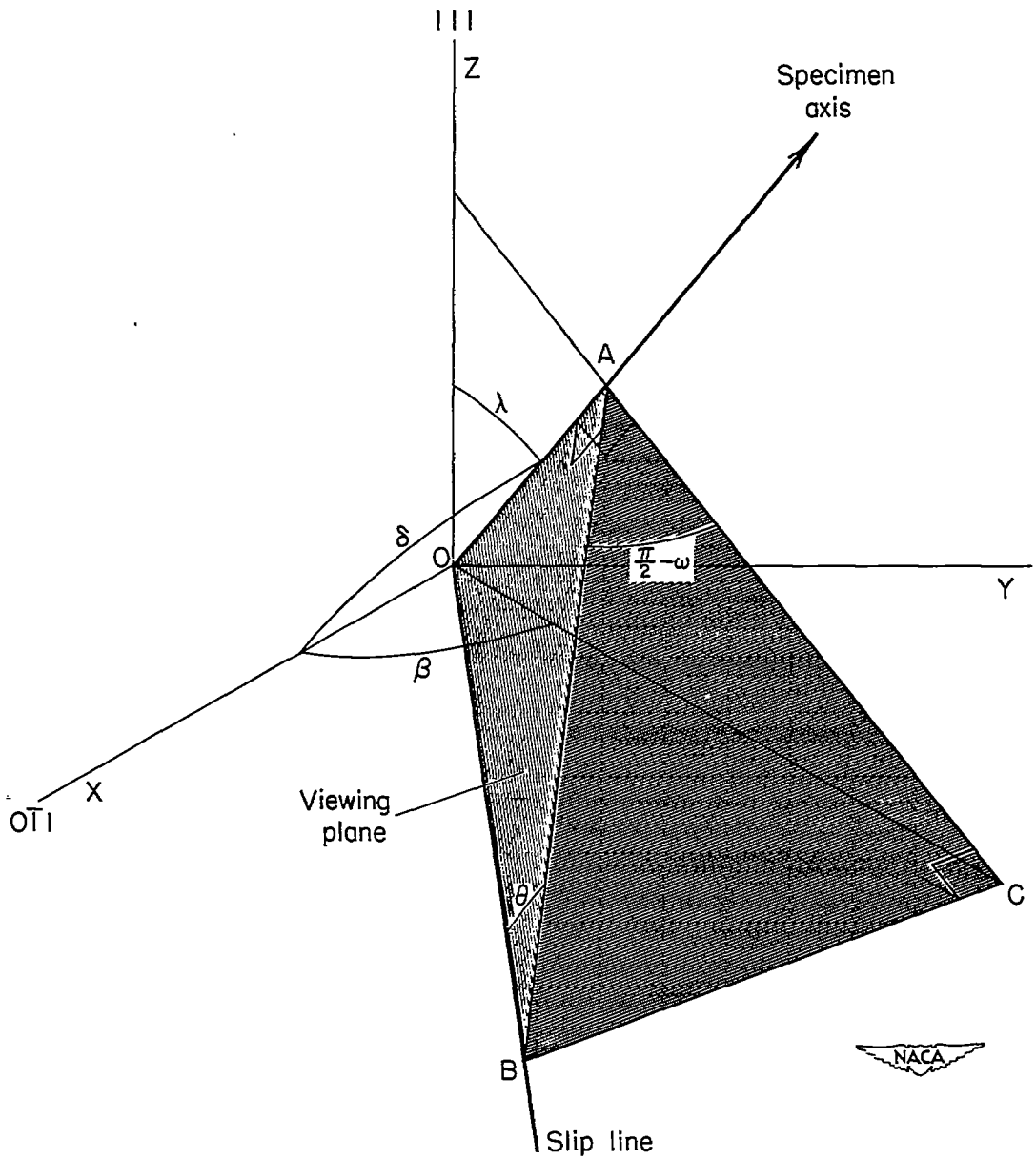

Figure 3.- Geometry of the planes, directions, and angles involved in the analysis.

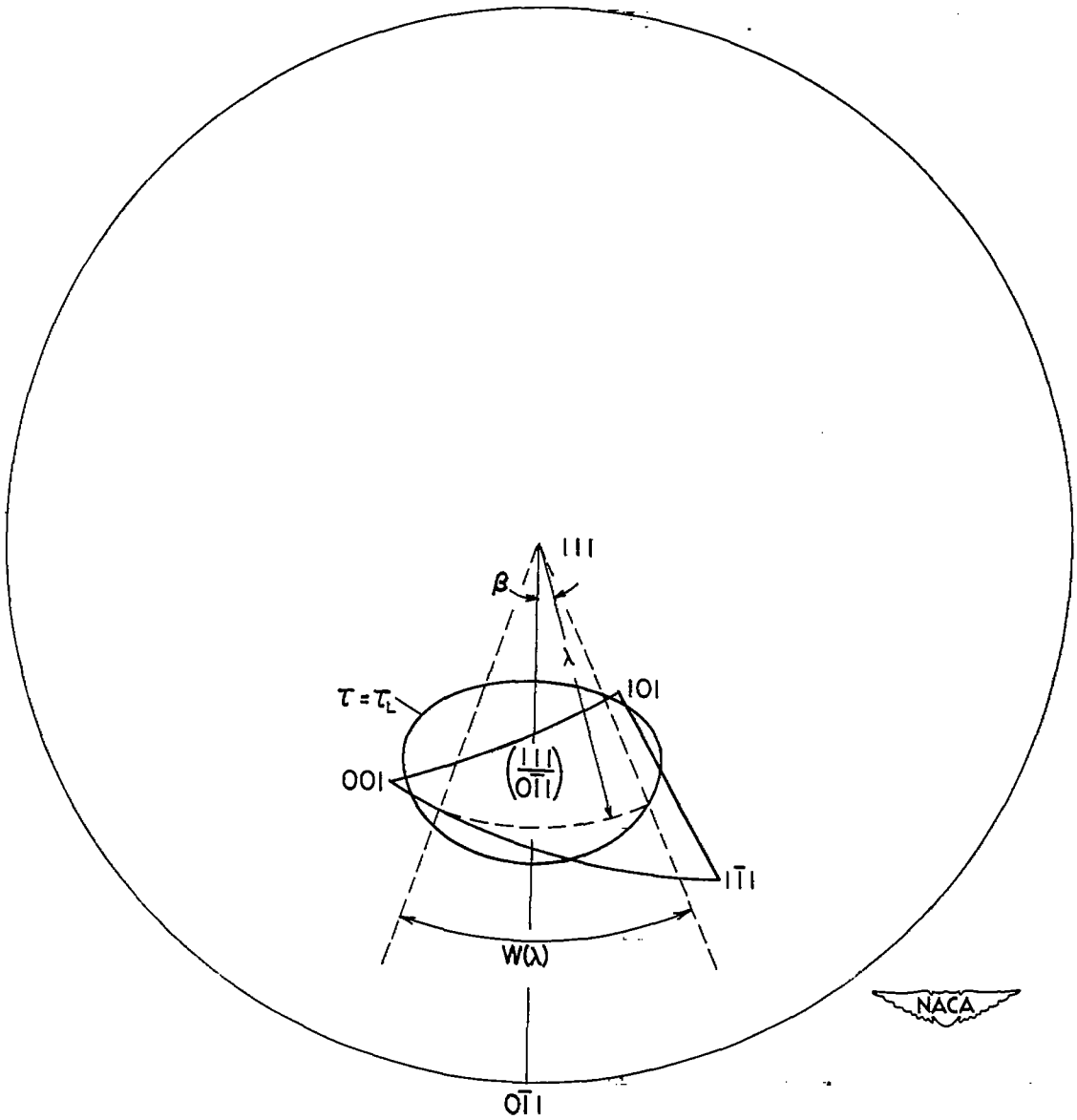

Figure 4.- Stereographic projection of the curve $\tau = \tau_L$ superimposed on the particular spherical triangle of interest.

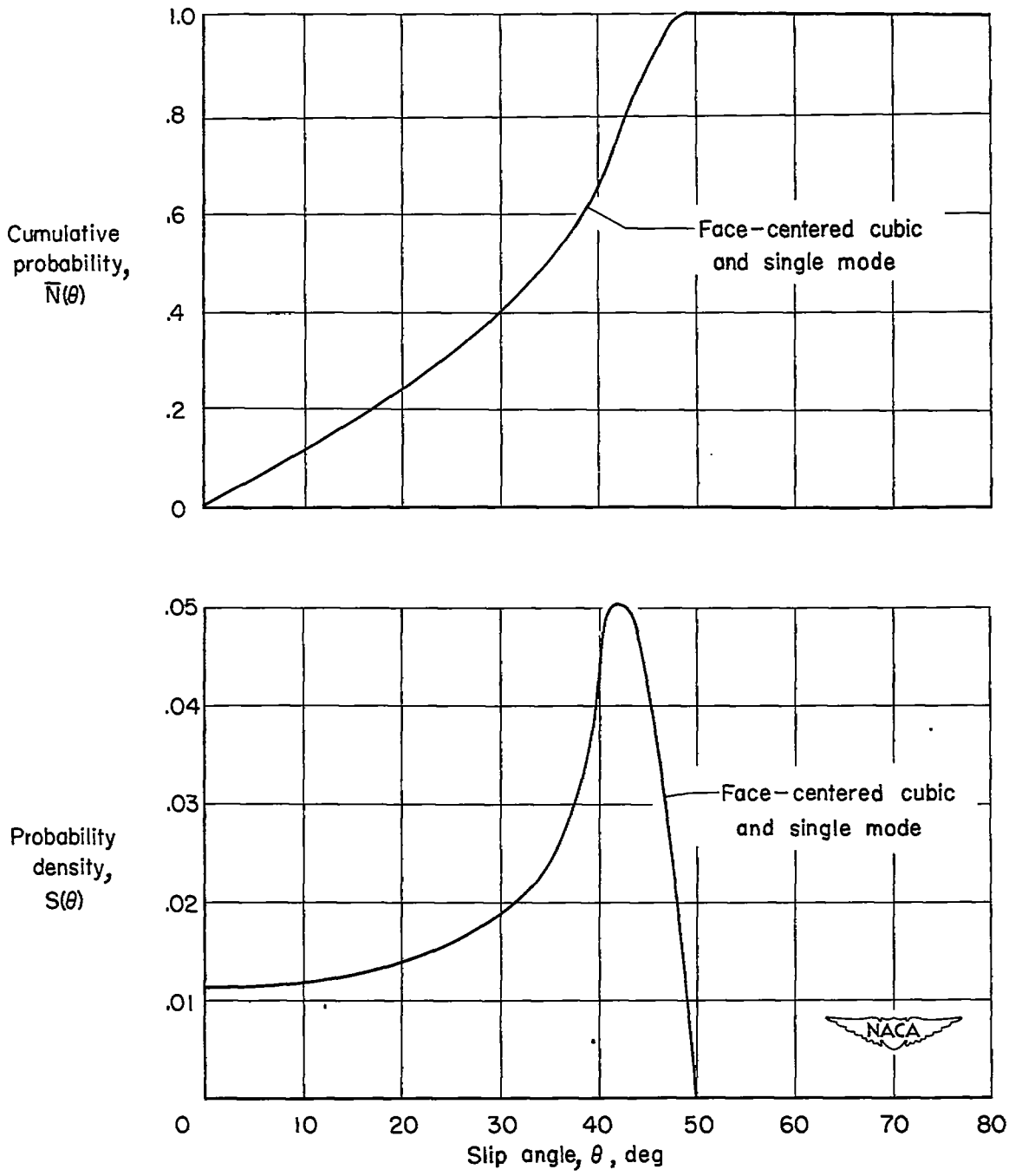

Figure 5.- Slip-angle distribution for stress ratio R = 1.015.

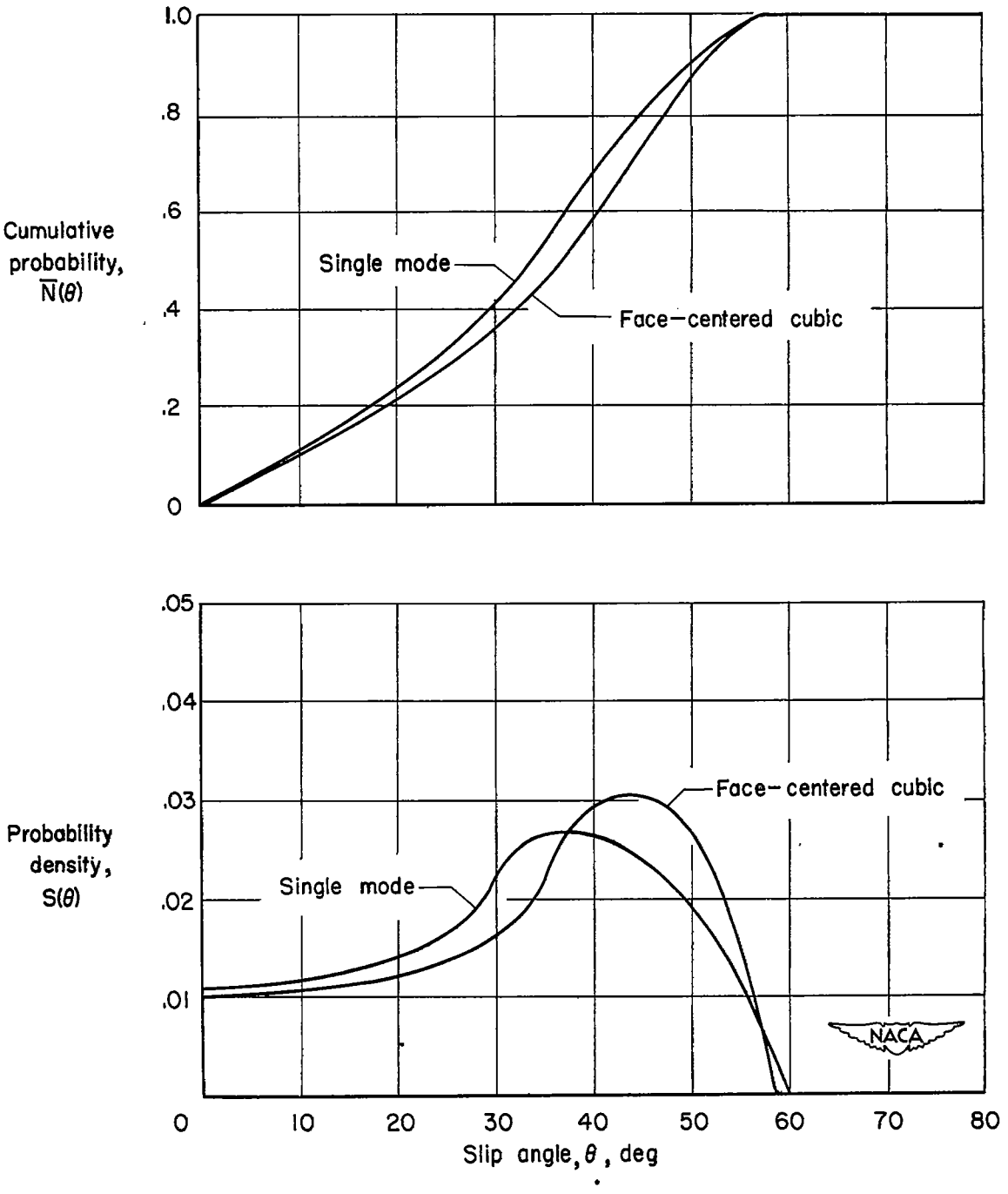

Figure 6.- Slip-angle distribution for stress ratio R = 1.156.

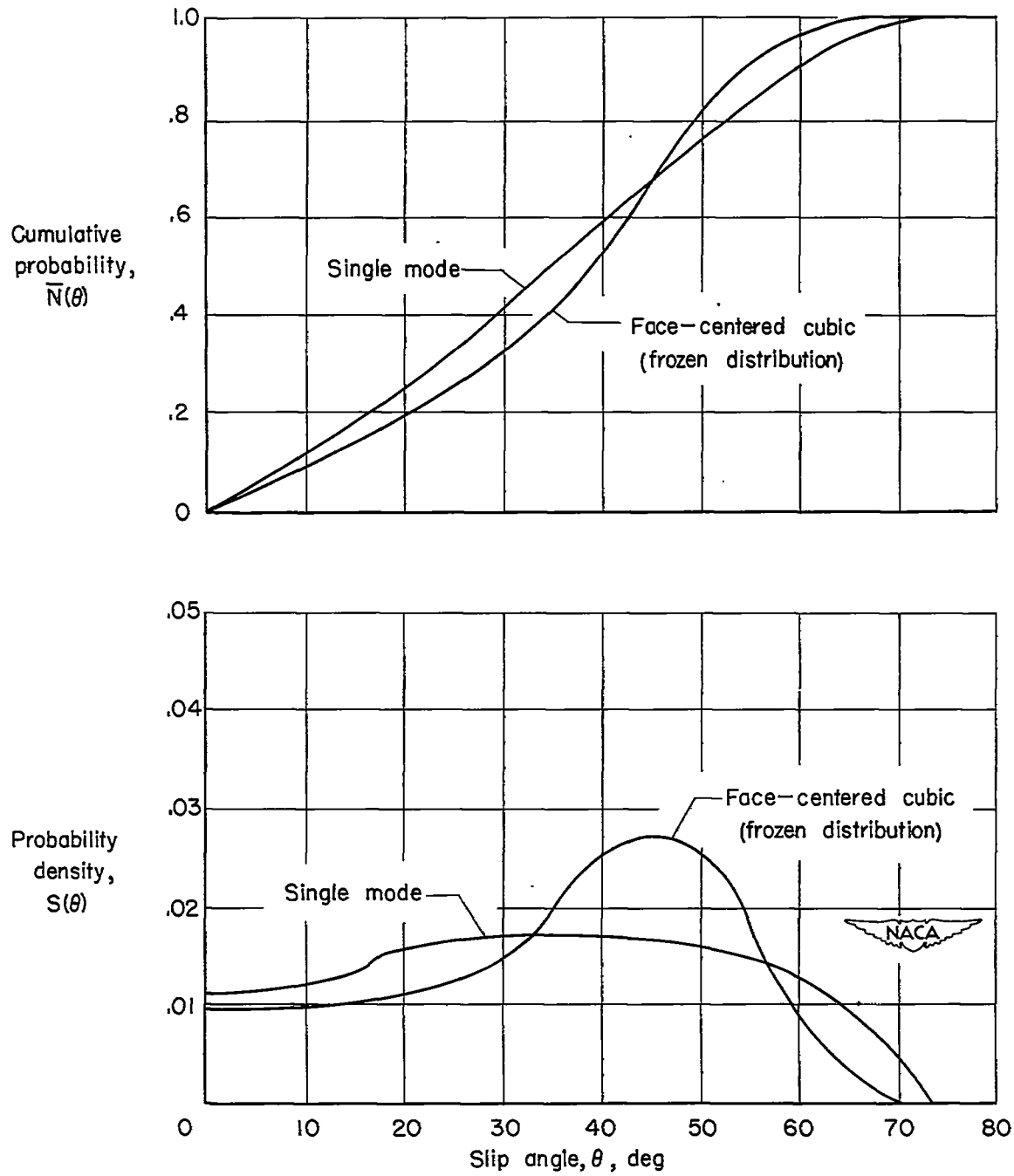

Figure 7.- Slip-angle distribution for stress ratio R = 1.837.

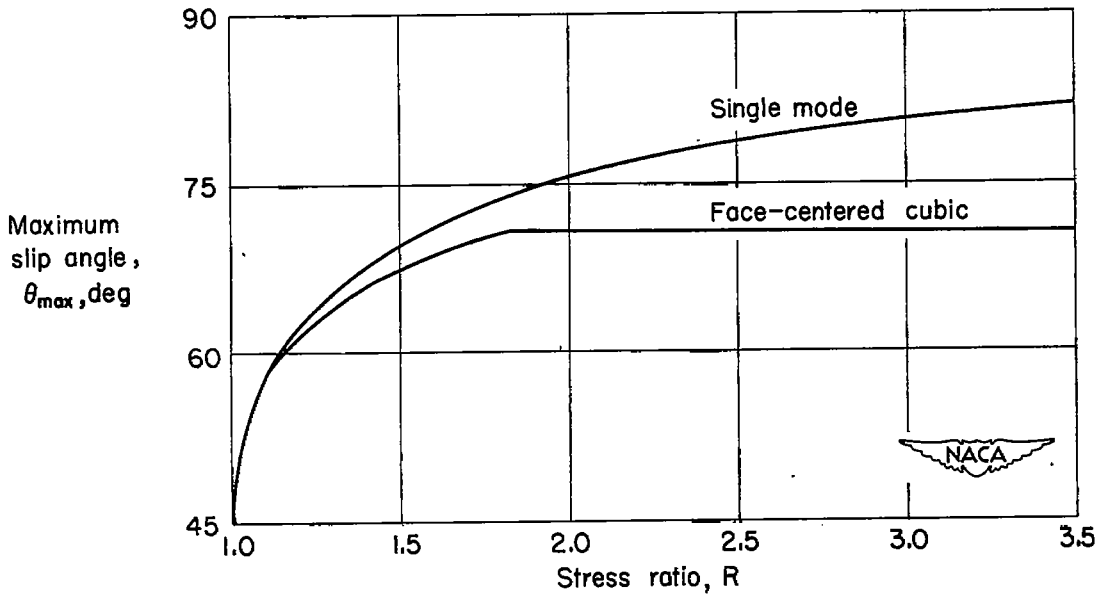

Figure 8.- Variation of maximum slip angle with stress ratio.

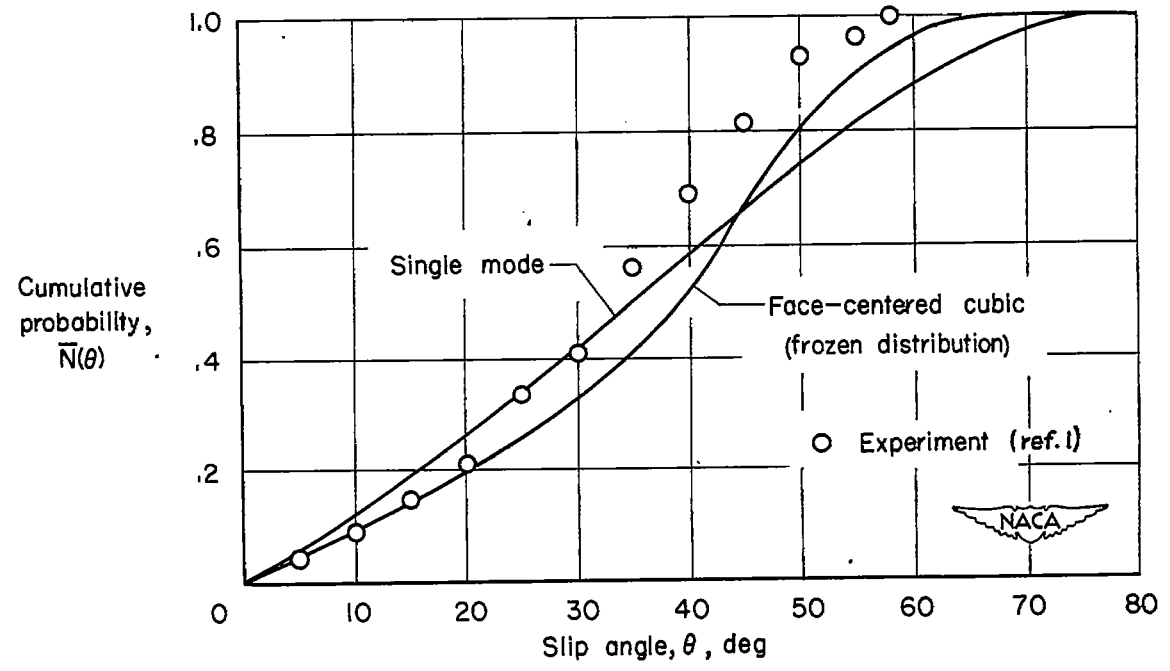

Figure 9.- Theoretical and experimental slip-angle distribution for stress ratio R = 2.000.

NACA-Langley - 8-28-52 - 1000